# Supporting information

## Atomic Force Microscopy-Based Top-Illumination Electrochemical Tip-Enhanced Raman Spectroscopy

Yi-Fan Bao,[†] Mao-Feng Cao,[†] Si-Si Wu,[†] Teng-Xiang Huang,*[,†] Zhi-Cong Zeng,[‡] Mao-Hua Li,[†] Xiang Wang,[†] and Bin Ren*[,†]

[†]State Key Laboratory of Physical Chemistry of Solid Surfaces, Collaborative Innovation Center of Chemistry for Energy Materials (*i*ChEM), College of Chemistry and Chemical Engineering, Xiamen University, Xiamen 361005, China

[‡]College of Chemistry and Chemical Engineering, Lanzhou University, Lanzhou, Gansu 730000, P. R. China.

*Bin Ren: bren@xmu.edu.cn

*Teng-Xiang Huang: txhuang@xmu.edu.cn

## Table of Contents

## 1. Top-illumination EC-AFM-TERS setup

Figure S1 illustrates the configuration of our top-illumination EC-AFM-TERS setup. The setup is on the basis of a commercial TERS system, which couples the commercial AFM module with a confocal Raman spectroscopy module. The Raman spectroscopy module uses the 632.8 nm He-Ne laser as the incident light. The incident laser is coupled with the TERS tip through the 100× water immersion objective. Afterwards, the back scattered Raman signal is collected with the same objective and passes through two edge filters. Finally, the Raman signal is dispersed by the spectrograph and detected with an EMCCD.

Besides, a white light optical imaging module is coupled in the TERS system to acquire a high-quality white light image. An electrochemical control module mainly consists of a potentiostat that is connected with the sample via Au leads to control the potential.

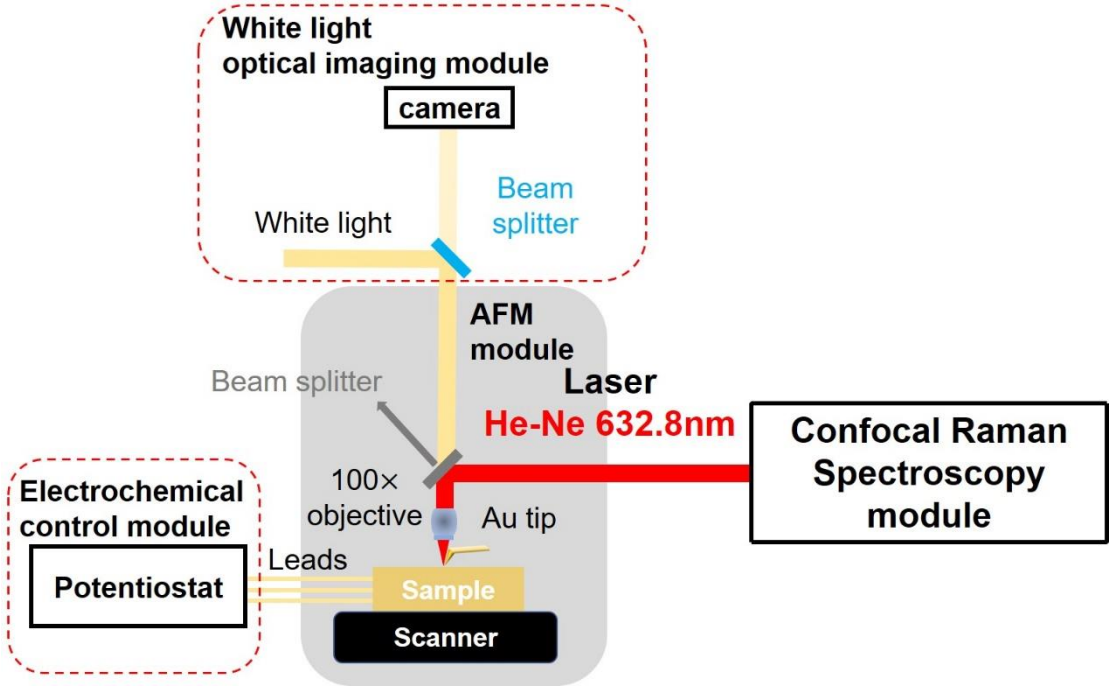


Figure S1. Schematic diagram of the top-illumination EC-AFM-TERS setup, including modules of Raman spectroscopy, SPM, white light optical microscope, and the electrochemical control.

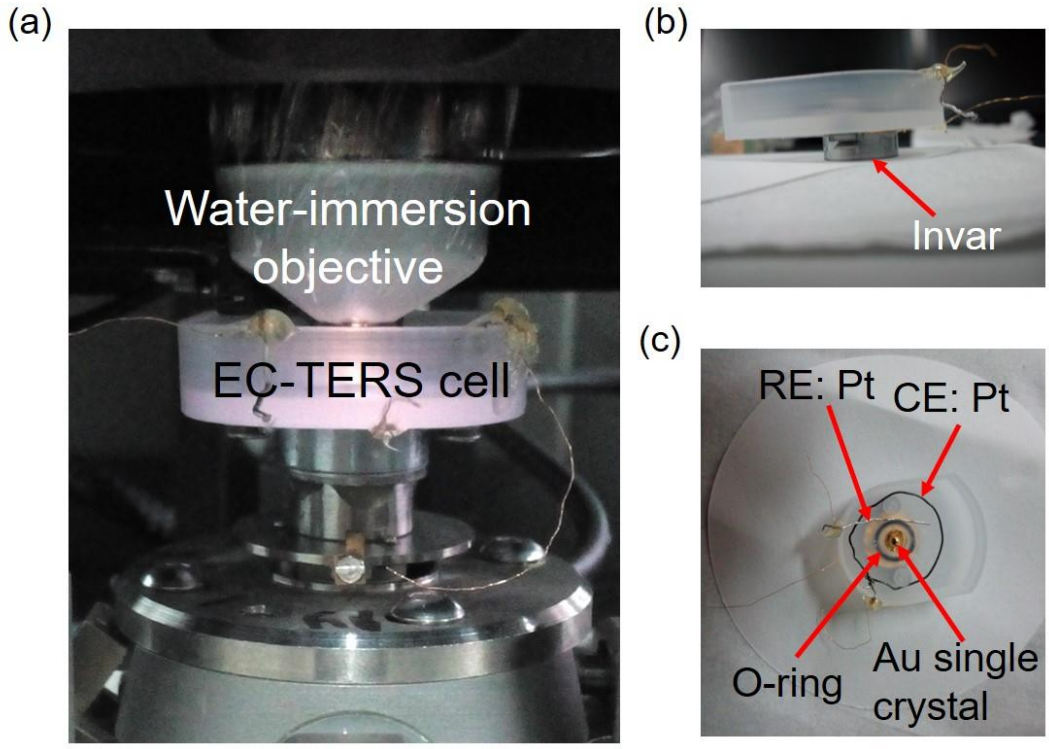


Figure S2. Photos of the top-illumination EC-TERS setup. (a) Photo of the water-immersion objective (covered with a PE film for protection) and the EC-TERS cell installed in the AFM module. (b) Side view of the EC-TERS cell mounted on an invar support. (c) Top view of the EC-TERS cell. A Au single crystal was used as the working electrode (WE), a Pt wire as the quasi reference electrode (RE), and a Pt ring as the counter electrode (CE). An O-ring is was mounted between the Au single crystal and the hole to avoid the leakage of the electrolyte.

## 2. Tapping mode AFM in liquid

Figure S3 illustrates the resonant frequency peaks of the AFM tip in air and liquid. Only one peak from the tip with a high signal to noise ratio is observed in air (Figure S3(a)). However, a lot of resonant peaks are observed in water (Figure S3(b)). In order to identify the origin of these peaks, we acquired resonant frequency spectra of three different tips in water (Figure S3(c)). Several peaks located at the low frequency range (yellow background) could be detected for the three tips, which are from the resonant peaks of water and the resonant peaks of the tip holder. Moreover, the broad and blunt peaks (marked by the blue background), which has no consensus on their origin, should not be chosen since they are less sensitive to the AFM feedback. As each AFM tip may have a different resonant frequency (e.g., 90~125 kHz for tip 3), we have to follow the following protocol to find the suitable peak for EC-TERS. First, different tips have different resonant peaks, the peak always appears at the same frequency for different tips may not from the tip. Second, the real resonant peak has a narrow shape with a medium intensity (the strongest peak does not work for approaching). Finally, the tip-sample approaching curve is used to judge the real resonant peak. For a suitable resonant peak (marked with green "*" in Figure S3(c)) from the tip, a upward shift of the oscillation in the tip-sample

approaching curve will be observed (Figure S3(d)). Whereas, there will be no upward shift in the curves of other resonant peaks (Figure S3(e))[1].

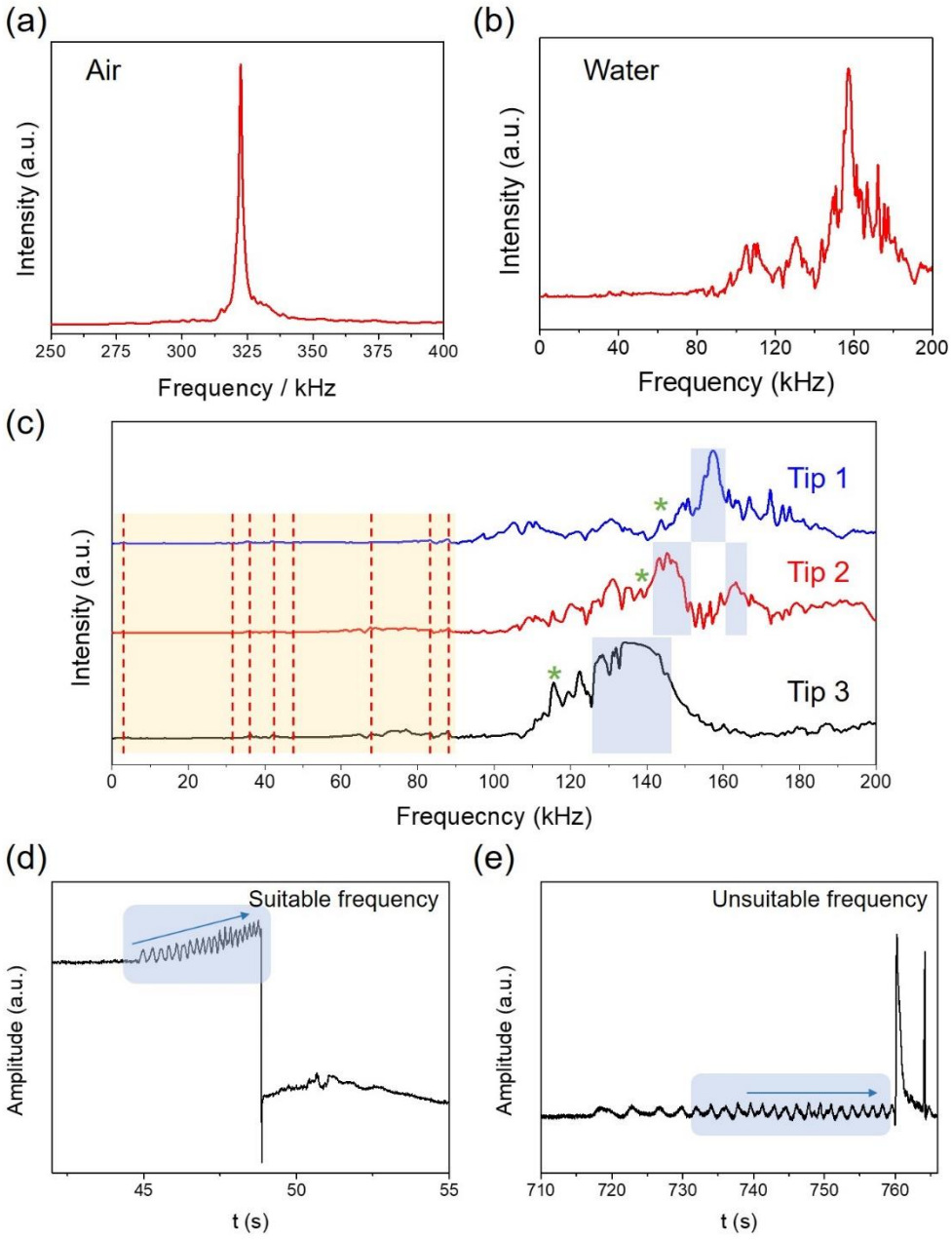


Figure S3. Typical resonant frequency curves of an AFM tip (VIT_P/IR, NT-MDT) in air (a) and liquid (b). (c) Resonant frequency spectra of three AFM tips in water. Tip-sample approaching curves of the same AFM tip with a suitable resonant frequency (d) and unsuitable resonant frequency (e).

## 3. Cyclic voltammetry (CV) characterization with the EC-TERS cell

The electrochemical performance of the EC-TERS cell was characterized by CV. A Au film

with a thickness of 200 nm was used as WE, a Pt ring was used as CE and a Pt wire was used as the quasi reference electrode. The electrolyte consists of 10 mM $K_4Fe(CN)_6$, 10 mM $K_3Fe(CN)_6$ and 0.5 M KCl. The result was shown in Figure S4. The $\Delta E_p$ = 90 mV, which is larger than the theoretical value (57mV) for a reversible redox system. This difference mainly comes from the iR drop as a result of the solution resistance.

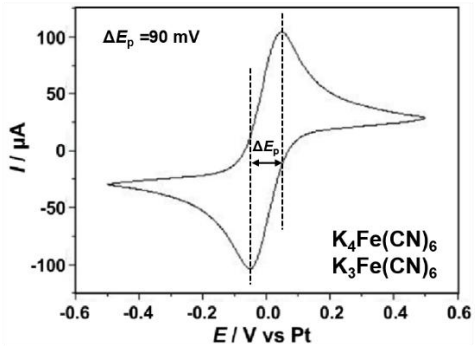


Figure S4. CV result obtained in the EC-TERS cell. WE: 200 nm-thick Au film. CE: Pt ring. RE: Pt wire. Electrolyte: 10 mM $K_4Fe(CN)_6$ + 10 mM $K_3Fe(CN)_6$ + 0.5 M KCl.

## 4. Comparison of the Au TERS tip and the $SiO_2$/Au TERS tip

To give a more quantitative comparison the S/N ratio (SNR) of the 1577 $cm^{-1}$ in air and in water，SNR is calculated by the following equation:

$$\mathrm{SNR} = \frac{S}{\sigma}$$

where $S$ is the peak height after baseline subtraction, $\sigma$ is the standard deviation of the noise[2]. The calculated SNR are listed in Table S1.

Table S1 Calculated SNR of TERS spectra

| TERS spectra | SNR |
|---|---|
| Bare Au tip TERS in air (Figure 2a black) | 67 |
| Bare Au tip TERS in water (Figure 2a red) | 11 |
| $SiO_2$/Au tip TERS in air (Figure 2b red) | 45 |
| $SiO_2$/Au tip TERS in water (Figure 2b blue) | 59 |

We then calculated the SNR of the 1577 $cm^{-1}$ peak by using five different Au tips and $SiO_2$/Au tips and the statistic SNR is shown in Figure 2(c).

## 5. Characterization of the Au TERS tip after the liquid TERS

Figure S5 shows a typical SEM image of the Au TERS tip after TERS measurement in water. We could not observe any obvious delamination and abrasion of the Au layer. We propose that there could be some small, even atomic scale features at the tip apex that have been abraded in liquid but could not be observed in SEM.

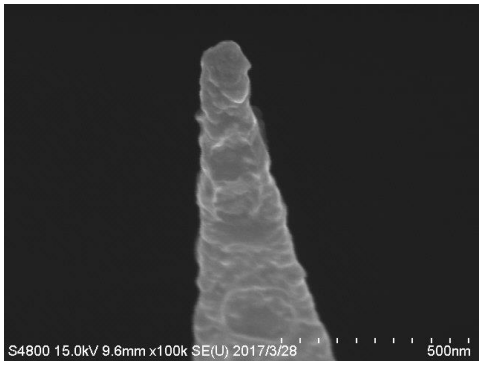


Figure S5. SEM image of the Au-coated AFM-TERS tip after the TERS measurement in water.

## 6. Characterization of the $SiO_2$ thickness grown by ALD

Since it is difficult to directly characterize the thickness of the $SiO_2$ layer over the Au-coated AFM-TERS tips, we estimate the thickness from the relationship between the thickness and the ALD cycle number on a Au film as schematically shown in Figure S6(a). First, ~200 nm Au layer was deposited on the Si substrate without any buffer layer. After the removal of part of the Au layer by a tape, the substrate was used for the ALD growth of $SiO_2$. Afterward, the remained Au layer with a $SiO_2$ layer was peeled off with a tape, exposing the edge of the $SiO_2$ layer on the Si surface. Finally, we obtained the thickness of the $SiO_2$ layer by measuring this edge by AFM. By increasing the ALD cycles (five, seven, and nine cycles), a working curve between the thickness and the ALD cycles could be obtained, as shown in Figure S6(b). We speculated the thickness of the $SiO_2$ layer (5-6 ALD cycles) in our experiment to be around 0.7-1.0 nm from the working curve.

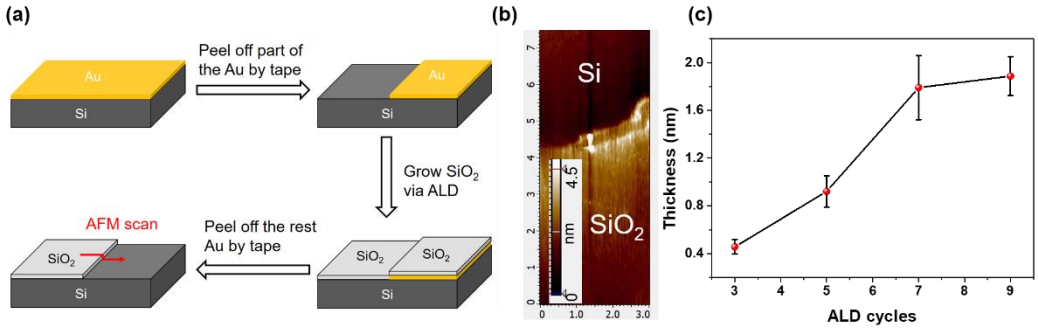


Figure S6. (a) Schematic of the AFM characterization of the thickness of ALD grown $SiO_2$ layer. (b) AFM image of the step. (c) The working curve of the ALD grown $SiO_2$ thickness and ALD cycles. Error bars indicate the standard derivation.

## 7. Characterization of the PANI coated Au film

Figure S7 shows the AFM image of the 2.2 nm PANI coated Au film. This characterization confirmed that a smooth PANI layer could be obtained via the potentiostatic electropolymerization.

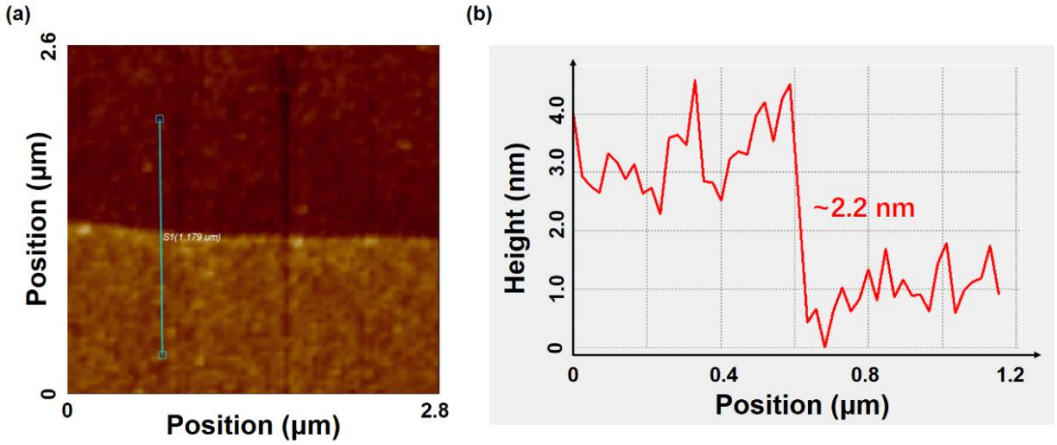


Figure S7. (a)AFM image of the 2.2 nm PANI coated Au film and (b) the height profile of the green line shown in (a).

Figure S8 shows the potential-dependent absorption spectra of the PANI coated Au film. During the experiment, under the white light illumination, we acquired the reflection spectra of a bare Au film ($R_{Au}$) at different potentials in 0.1 M HCl, which is used as the reference. We then acquired the reflection spectra of a PANI-coated Au film ($R_{Au\text{-}PANI}$) at different potentials in the same electrolyte. The absorbance ($A$) of PANI could be calculated by the following formula: $A=\frac{R_{Au}-R_{Au\text{-}PANI}}{R_{Au}}$.

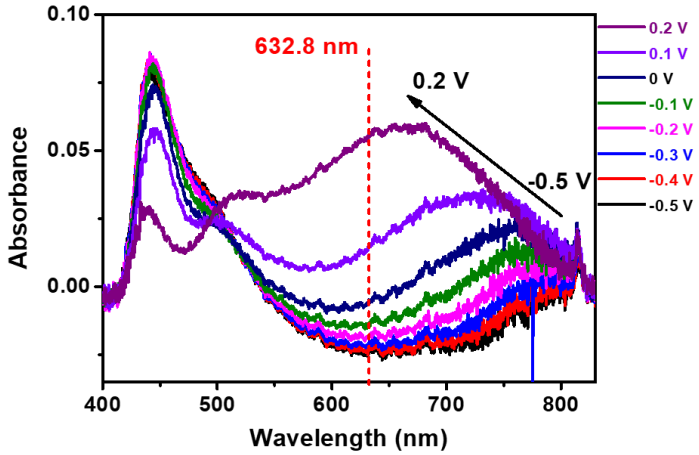


Figure S8. Potential-dependent absorption spectra of PANI in 0.1 M HCl. The absorption peak undergoes a blue shift with the increase of the potential. The absorption peaks of PANI shifts to 665 nm, which resonates with the 632.8 nm laser.

## 8. EC-AFM Imaging of PANI

EC-AFM imaging of PANI was performed with the same setup as EC-AFM-TERS except for the use of commercial Si AFM tip and working in AFM tapping mode. The potential was swept from -0.4 V to 0.3 V and back to -0.4 V. Figure S9 and Figure S10 show the potential-dependent AFM images and thickness of PANI on Au film in 0.1 M HCl solution, respectively. The thickness of the PANI first gradually increases and then decreases with the increase of potential.

This is because of the intercalation and deintercalation of $Cl^-$ within the matrix of PANI[3]. As shown in Figure S11[4], when a negative potential is applied to the PANI layer, PANI is in a full-reduced state consisting of benzenoid, and no $Cl^-$ ions intercalation occurs. However, when the pH of the solution is lower than 3 (pH=1 in our experiment), a small number of C-N- sites will be protonated, so that a very few amounts of $Cl^-$ may intercalate into these sites. With the increase of the potential, the partially protonated PANI will be converted to the salt form of emeraldine (SQ) (Figure S11, Half-oxidized state). Four structural units may exist and the most stable one is the polaron lattice. With the further increase of the potential, the PANI becomes a full-oxidized state consisting of quinoid ring. No $-C-N^+$ structure exists, leading to the deintercalation of $Cl^-$. part of the C-N- sites is still protonated at such a low pH, so a very few amounts $Cl^-$ may intercalate into the polymer. Therefore, the thickness of PANI layer firstly increases and then decreases due to the intercalation and deintercalation of $Cl^-$ ions during the positive scan. Similar phenomenon was observed during the reverse scan.

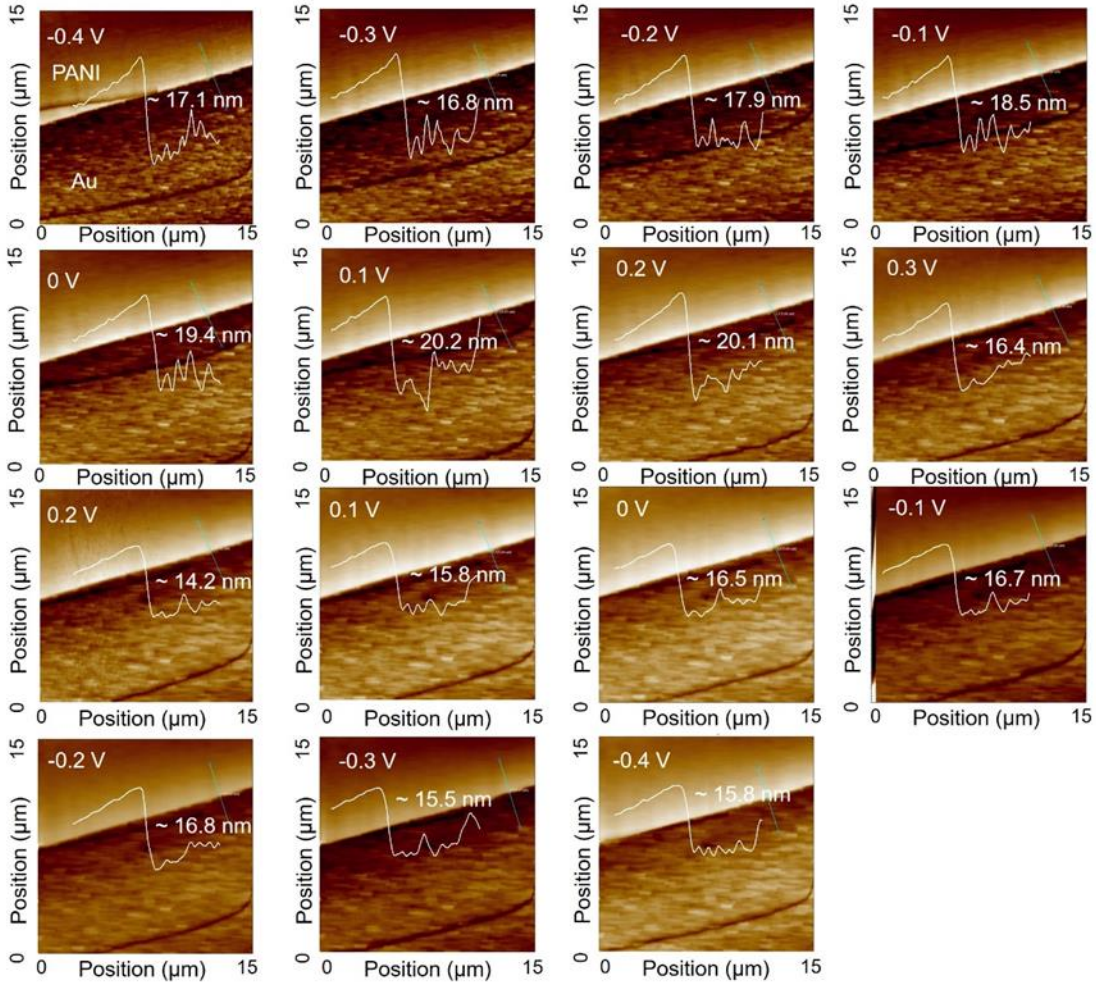


Figure S9 In-situ EC-AFM images of the PANI coated Au film in 0.1 M HCl solution. Note that the curvy moving feature at the lower right edge is the artifact of the scanner.

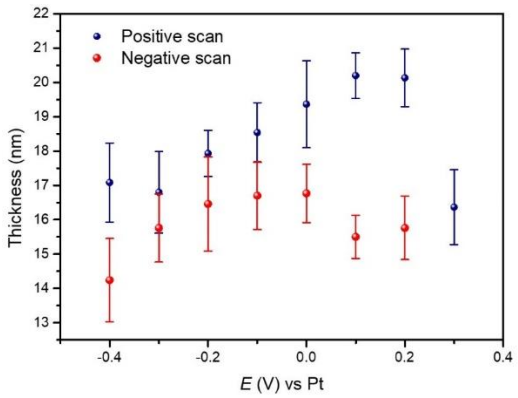


Figure S10 Potential dependent thickness of the PANI layer. Error bars indicate the deviation of the thickness at different potentials.

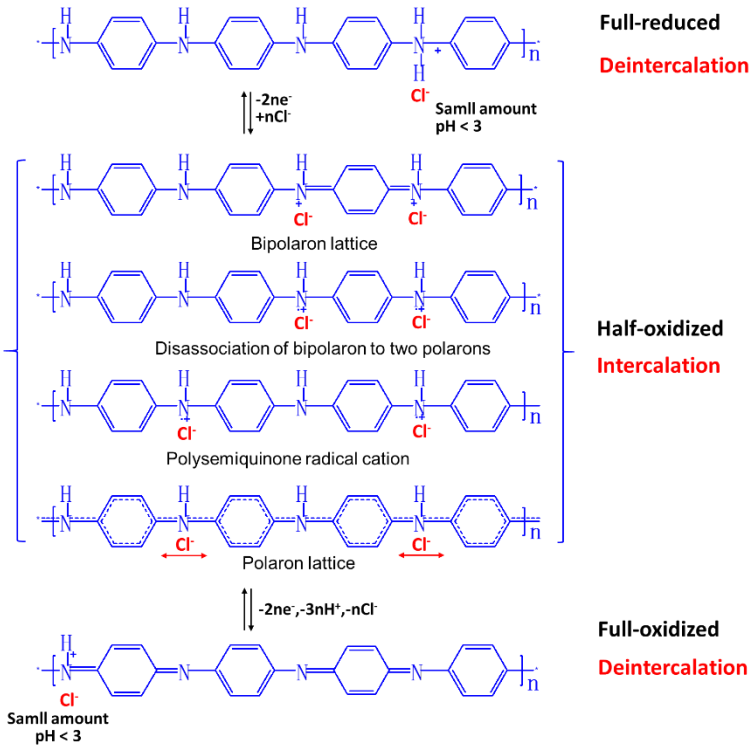


Figure S11 Illustration of the intercalation and deintercalation of anion during the redox process of PANI.

## 9. Potential dependent TERS spectra of PANI on Au film

Figure S12 shows the complete potential-dependent TERS spectra of PANI. It clearly shows that leucoemeraldine is gradually oxidized to pernigralldine when the potential sweeps from -0.3 V to 0.3 V, and pernigralldine is reversibly reduced to leucoemeraldine when the potential sweeps back to -0.3 V. As the potential sweeps back from 0.3 V to -0.3 V, the intensity decreased a little, which may come from the degradation of some polymer after long time exposure to the laser.

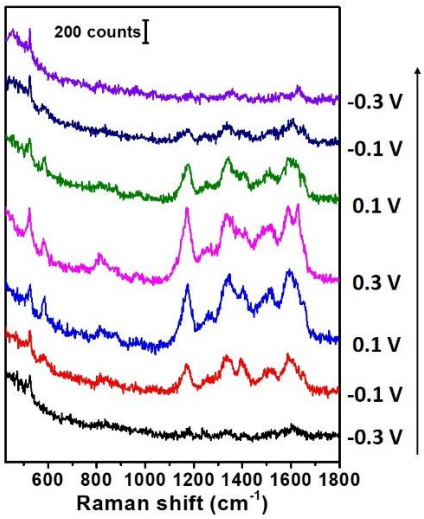


Figure S12. Potential-dependent TERS spectra of PANI on Au in 0.1 M HCl solution from -0.3 V to 0.3 V and back to -0.3 V.

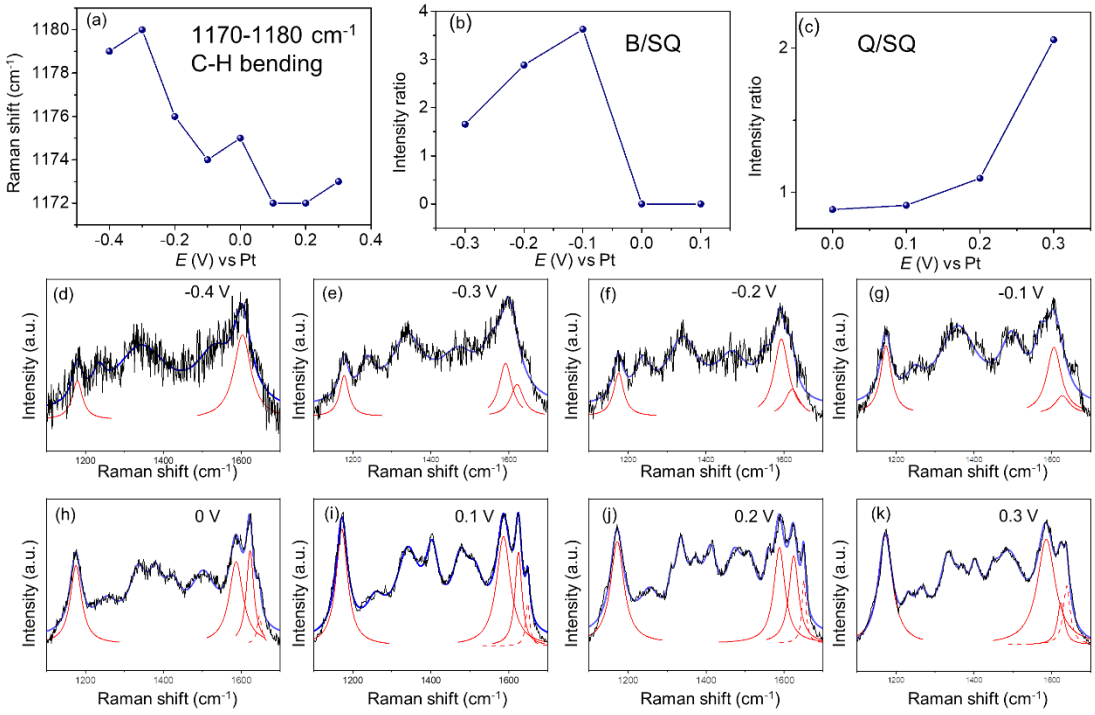


Figure S13 (a) The plot of the TERS peak position (1170-1180 $cm^{-1}$) change against the potential. (b) The plot of TERS intensity contrast of C-C stretching of B (1590-1610 $cm^{-1}$) and C-C stretching, SQ (16220-1640 $cm^{-1}$) against potential. (c) The plot of the TERS intensity contrast of C=C stretching of Q (1580-1590 $cm^{-1}$) and C-C stretching of SQ (16220-1640 $cm^{-1}$) against potential. (d)-(k) Lorentzian fitting results of the TERS spectra mentioned in the main text. Black lines: original data. Blue lines: Lorentzian of the EC-TERS spectra from 1100 $cm^{-1}$ to 1700 $cm^{-1}$. Red lines: Lorentzian fits of the mentioned peaks. Red dash lines: Lorentzian fits of the not mentioned peaks.

The TERS spectra from 1100 $cm^{-1}$ to 1700 $cm^{-1}$ of PANI is quite complex, we focus on 4 peaks

(C-H bending of B or Q at 1170-1180 $cm^{-1}$, C-C stretching of B at 1590-1610 $cm^{-1}$, C=C stretching of Q at 1580-1590 $cm^{-1}$, C-C stretching of SQ at 16220-1640 $cm^{-1}$)[3,5,6] and use Lorentzian fits to better discuss these peaks. The fits results are shown in Figure S13 (d) to (k) and we listed the fits results in Table S2.

Table S2 Lorentzian fits results of the mentioned Raman peaks in main text

| *E*(V) vs Pt | C-H bending of B or Q (1170-1180 $cm^{-1}$) | | C-C stretching of B (1590-1610 $cm^{-1}$) | | C=C stretching of Q (1580-1590 $cm^{-1}$) | | C-C stretching of SQ (16220-1640 $cm^{-1}$) | |
|---|---|---|---|---|---|---|---|---|
| | Position ($cm^{-1}$) | Intensity (counts) | Position ($cm^{-1}$) | Intensity (counts) | Position ($cm^{-1}$) | Intensity (counts) | Position ($cm^{-1}$) | Intensity (counts) |
| -0.4 | 1179 | 62 | 1603 | 135 | N/A | N/A | N/A | N/A |
| -0.3 | 1180 | 83 | 1592 | 116 | N/A | N/A | 1622 | 70 |
| -0.2 | 1176 | 126 | 1592 | 225 | N/A | N/A | 1621 | 78 |
| -0.1 | 1174 | 281 | 1605 | 272 | N/A | N/A | 1636 | 75 |
| 0 | 1175 | 593 | N/A | N/A | 1586 | 623 | 1622 | 707 |
| 0.1 | 1172 | 1428 | N/A | N/A | 1587 | 1043 | 1625 | 1145 |
| 0.2 | 1172 | 1126 | N/A | N/A | 1587 | 1061 | 1625 | 966 |
| 0.3 | 1173 | 1997 | N/A | N/A | 1584 | 1955 | 1622 | 950 |

## Reference


(1) Putman, C. A. J.; Werf, K. O. V. d.; Grooth, B. G. D.; Hulst, N. F. V.; Greve, Tapping Mode Atomic Force Microscopy in Liquid. J. *Appl. Phys. Lett.* **1994**, *64*, 2454-2456.

(2) Etchegoin, P. G.; Le Ru, E. C. A Perspective on Single Molecule SERS: Current Status and Future Challenges. *Phys. Chem. Chem. Phys.* **2008**, *10*, 6079-6089.

(3) Jiao, L.-S.; Wang, Z.; Niu, L.; Shen, J.; You, T.-Y.; Dong, S.-J.; Ivaska, A. In Situ Electrochemical SERS Studies on Electrodeposition of Aniline on 4-ATP/Au Surface. *J. Solid State Electr.* **2006**, *10*, 886-893

(4) Ping, Z.; Gerhard E. Nauer, B.; Neugebauer, H.; Theiner, J.; Neckel, A., Protonation and Electrochemical Redox Doping Processes of Polyaniline in Aqueous Solutions: Investigations Using in situ FTIR-ATR Spectroscopy and A new Doping System. *J. Chem. Soc., Faraday Trans.* **1997,** *93*, 121-129.

(5) Lapkowski, M.; Berrada, K.; Quillard, S.; Louarn, G.; Lefrant, S.; Pron, A. Electrochemical Oxidation of Polyaniline in Nonaqueous Electrolytes: "In Situ" Raman Spectroscopic Studies. *Macromolecules* **1995**, *28*, 1233-1238.

(6) Liu, C.; Zhang, J.; Shi, G.; Chen, F. Doping Level Change of Polyaniline Film During Its Electrochemical Growth Process. *J. Appl. Polym. Sci.* **2004**, *92*, 171-177.